Tribology International 147 (2020) 105557

Contents lists available at ScienceDirect

Tribology International

journal homepage: www.elsevier.com/locate/triboint

Effect of mesh structure of tetrahedral amorphous carbon (ta-C) coating on friction and wear properties under base-oil lubrication condition☆

Mohd Muhyiddin Bin Mustafa[a,c,*], Noritsugu Umehara[a], Takayuki Tokoroyama[a], Motoyuki Murashima[a], Akinori Shibata[b], Yoshiharu Utsumi[b], Hideki Moriguchi[b]

[a] Department of Micro-Nano Mechanical Science and Engineering, Graduate School of Engineering, Nagoya University, Furo-cho, Chikusa-ku, Nagoya, Aichi 464-8603, Japan
[b] Technology Development Center, Nippon ITF Inc., 47, Umezu-Takase-cho, Ukyo-ku, Kyoto 615-8686, Japan
[c] Faculty of Mechanical and Manufacturing Engineering Technology, Universiti Teknikal Malaysia Melaka, Hang Tuah Jaya, 76100 Durian Tunggal, Melaka, Malaysia

ARTICLE INFO

Keywords:
Friction
Wear
Diamond-like carbon
Material structure

ABSTRACT

This study examined the tribological properties of novel mesh tetrahedral amorphous carbon (Mesh ta-C). Subsequently, comparison was made with conventional ta-C and a-C:H coatings under base-oil lubrication via cylindrical-pin-on-disk tribo-tester. Analysis of wear track was conducted using field-emission-scanning-electron-microscope (FE-SEM), atomic-force-microscopy (AFM), and Raman-spectroscopy. The friction coefficient for Mesh ta-C and conventional ta-C revealed a similar pattern with regard to loads. The Mesh ta-C had excellent wear resistance, where the wear rates at loads of 20 N was five and 20 times lower than conventional a-C:H and ta-C, respectively. High wear resistance of Mesh ta-C characterized by inhibition of brittle micro-fracture propagation, less in abrasive particle created during friction test, and suppressing the effect of graphitization-induced wear on the contact surface.

1. Introduction

Diamond-like carbon (DLC) coatings are known as remarkable features applied as the solid lubricants because of low friction, high hardness as well as wear resistance and chemical inertness. Presently, the DLC coating has been widely utilized in various industrial applications to reduce friction and wear, particularly in the automotive industry. As such, this industry continuously is pursuing lower energy loss and low gas emissions. In order to achieve legal regulations in relation to energy efficiency and greenhouse gas emissions, DLC coatings could be a promising surface material applied on extremely stressed components of internal combustion engines to reduce friction and to extend component lifetime [1].

DLC is divided into two major categories, namely the hydrogenated amorphous carbon (a-C:H, ta-C:H) and the hydrogen-free amorphous carbon (a-C, ta-C). Both hydrogenated amorphous carbon (a-C:H) and hydrogen-free tetrahedral amorphous carbon (ta-C) coatings offer low friction performance and excellent wear resistance with diverse characteristics of friction and wear properties owing to their particular hydrogen contents and microstructure [2]. Friction and wear sensitively rely upon system encompassing surface material, lubricants (oil and additive), environment (temperature, humidity) and lubrication condition [1–10]. It should be noted that most engine components are operated in the boundary lubrication regime. Under moderately severe contact conditions in boundary lubrication regime, direct contact occurs between the sliding surfaces.

Numerous studies have conducted the friction test under the boundary lubricated regime for DLC coating [11–14]. Nevertheless, many researchers studied the effect of different lubricating oil and additive to the tribological performance of the DLC coatings. Under appropriate base oil and lubricant additives, the tribological performance of various types of DLC coating provides ultra-low friction and high wear resistance [15]. Oil additives and DLC doping elements demonstrated substantial and valuable impact on the wear behaviour [11,16]. Nonetheless, evidence has shown that the use of oil additives containing phosphorus and sulfur results in substantial harmful effect to the environment upon refinement process [17].

High hardness material commonly provides a higher wear resistance compared to the low hardness material under moderate experimental setup. Nevertheless, with a severe condition, hard and brittle material

☆ This paper was presented at the ASIATRIB2018.

* Corresponding author. Department of Micro-Nano Mechanical Science and Engineering, Graduate School of Engineering, Nagoya University, Furo-cho, Chikusa-ku, Nagoya, Aichi 464-8603, Japan.
E-mail address: muhyiddin@ume.mech.nagoya-u.ac.jp (M.M.B. Mustafa).

https://doi.org/10.1016/j.triboint.2019.01.016
Received 10 September 2018; Received in revised form 14 January 2019; Accepted 14 January 2019
Available online 30 January 2019
0301-679X/

with lesser crack resistance results in coating damage due to micro-fracture. Wear by means of fracture-induced, which has been regarded as significant wear mechanism of brittle material can increase approximately ten times compared to abrasive wear [18]. In the case of DLC coatings, wear is accelerated by the through-thickness crack that causes spalling of the coating [19]. Furthermore, low hardness coating that forms of high fraction sp^2 carbon atoms also results in high material removal rates under severe condition due to the structural modification such as graphitization of the contact surface [20,21]. The hardness of the DLC coating depends on the fraction of the sp^3 and sp^2 carbon structure [22].

Many studies have focused on the ta-C and a-C:H coatings, which demonstrated high wear or damage to the coating as the sliding distance, speed, temperature, and load are increased. According to a study by Ronkainen et al. [2], ta-C coating shows high wear resistance in contrast to the a-C:H, however, the ta-C coating created larger wear on the counterpart material. Superhard hydrogen free ta-C coatings are denoted by a high fraction of tetrahedral bonded (sp^3) carbon atoms [23]. A study by Al Mahmud et al. [10] revealed that the coefficient of friction (CoF) for both ta-C and a-C:H coatings decreased and largely affected by the coating graphitization that consequently increased the wear rates. This finding is in agreement with a previous study by Tasdemir et al. [9], where the ta-C coating had limited durability causing high wear rates at high temperature. In addition, ta-C performance also degraded due to an increase in the sliding distance and load when ta-C slides against steel in pure base oil lubrication due to fracture-induced wear. These led to coatings worn out due to polishing wear combined with tribo-chemical wear [6]. Notably, several studies have shown that a-C:H coating had larger wear rates under the similar experimental condition with ta-C coating [20,24].

Commonly, DLC is deposited with a layer of homogeneous structure except for multilayer coating design. The current research introduced and investigated a novel Mesh ta-C with as-deposited mesh structure. At present, investigation on the as-deposited coating structure and its influence on the tribological performance have been scant. Therefore, the current study is aimed to investigate the tribological features of the as-deposited mesh-type structure of tetrahedral amorphous carbon coating under base-oil lubrication conditions. Unlike the aforementioned DLC, Mesh ta-C coating properties are unique for its' mesh-like structure, which is characterized by the hardness controlled DLC in the direction of the coating thickness. This novel DLC consists of a softer topmost surface layer (sp^2–rich mesh structure) and hard substrate-side layer (sp^3–rich conventional ta-C), proposed to improve both friction and wear resistance of the coating.

2. Experimental details

2.1. Materials and lubricants

Cylindrical pin and disk were made of high carbon chrome steel (SUJ-2). Both forms of tetrahedral amorphous carbon (ta-C) and a type of hydrogenated amorphous carbon (a-C:H) were supplied by the Nippon ITF Inc. These two forms of ta-C were described by the structure, which are conventional tetrahedral amorphous carbon (ta-C) and mesh tetrahedral amorphous carbon (Mesh ta-C) deposited with mesh structure. The a-C:H coating was produced through chemical vapour deposition (CVD), while ta-C and Mesh ta-C coating were produced through physical vapour deposition (PVD). Additionally, fluid polishing was applied to remove the droplets on the coating surface originated from the deposition process, which could affect the tribological performance of the coating. The base-oil applied in this research was poly-alpha-olefin 4 (PAO4) with a viscosity of 6.11 mm^2/s and pressure-viscosity coefficient of 12.85 GPa^{-1} at 80 °C. The application of additive-free oil in this research permits the evaluation of the performance on the friction and wear of the DLC coating itself devoid of any impact from the additive in lubricant.

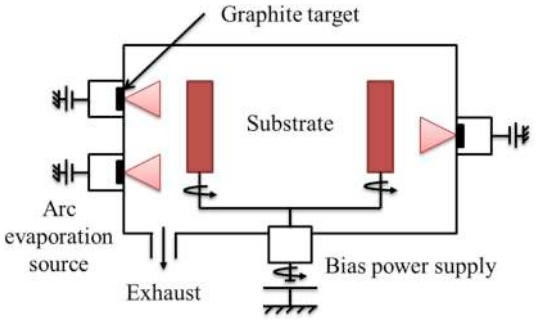

Fig. 1. Schematic diagram of arc PVD equipment [25].

2.2. Details characteristic of Mesh ta-C coating development

2.2.1. Deposition method and concept

Fig. 1 illustrates the arc PVD equipment used to deposit hydrogen free (H-free) DLC. Both conventional ta-C and newly developed Mesh ta-C DLC were deposited using the arc PVD equipment (M720) that could produce an arc discharge on a solid graphite target.

Typically, ta-C coating was deposited using the PVD method by controlling the deposition temperature below 150 °C by means of the cooling system during the coating growth as demonstrated in Fig. 2(a). Nevertheless, for the Mesh ta-C deposition process, the substrate was heated up from room temperature to 200 °C continuously during the deposition process as illustrated in Fig. 2(b). The hardness of the DLC coating decreased due to heating during the deposition process. By controlling the temperature distribution, the substrate-side coating is harder compared to the topmost surface coating. This feature is expected to reduce the effect of fracture-induced wear which is one of the reasons for ta-C coating high wear and short lifespan.

2.2.2. Coating structure

Transmission electron microscope (TEM) was used to observe the deposited ta-C and Mesh ta-C structure. Both samples were cut using a focused ion beam (FIB). Subsequently, the cross-sectional surface was observed using TEM H9000 UHR at an acceleration voltage of 300 kV. The TEM images of the conventional ta-C and Mesh ta-C are shown in Fig. 3.

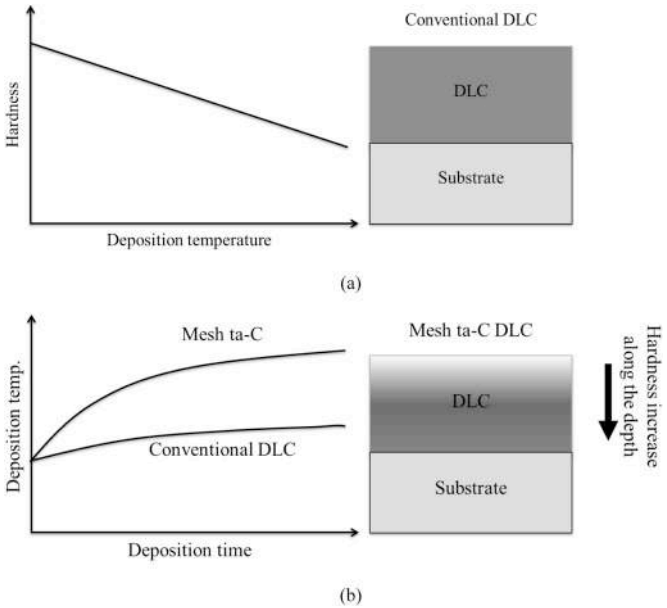

Fig. 2. Deposition method and material concept of (a) conventional ta-C, and (b) novel Mesh ta-C coating [25].

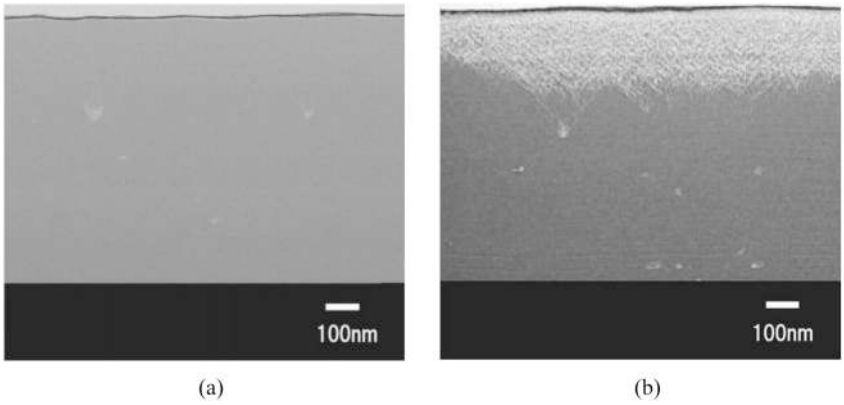

Fig. 3. Cross-sectional TEM images of (a) conventional ta-C, and (b) Mesh ta-C [25].

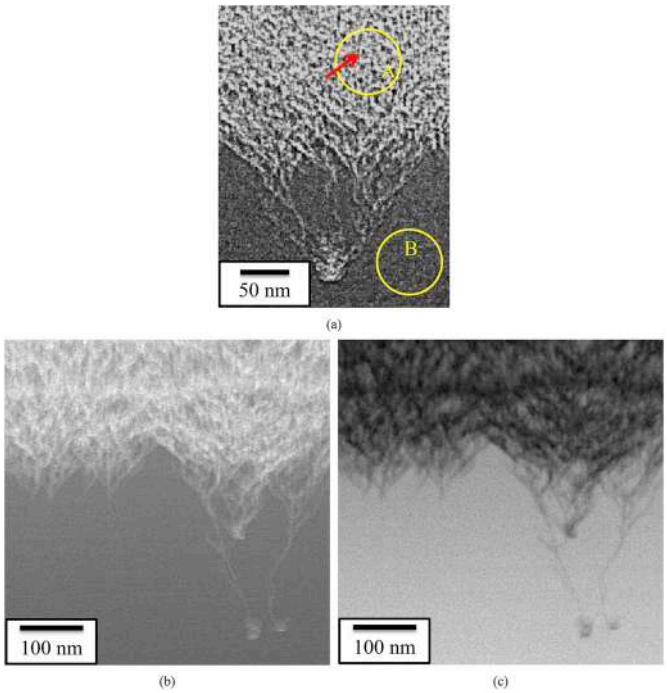

Fig. 4. Reticulated structure images of Mesh ta-C by (a) Magnified TEM [25], (b) bright-field scanning transmission electron microscopy (BF-STEM), and (c) high-angle annular dark-field scanning transmission electron microscopy (HAADF-STEM).

Fig. 3(a) demonstrates that the structure of conventional ta-C did not undergo changes from the substrate to the surface of the coating. The structure can be classified as homogenous despite the presence of some micro-particles. On the other hand, Mesh ta-C demonstrates a white layer that is located at a quarter of the coating thickness as observed in Fig. 3(b). Moreover, the magnified image of the white layer as shown in Fig. 4(a), (b), and (c), illustrates the reticulated structure growth from a microparticle, which is a feature of the arc technique applied for deposition.

The crystallinity analysis was conducted by electron diffraction method using Field Emission Electron Microscope JEM2100F, with 200 kV and 10^{-9} A acceleration voltage and absorbed current, respectively. Crystallinity assessment was performed at area A and B as demonstrated in Fig. 4(a), where there were two distinct structures observed. The results of electron diffraction in both areas are shown in Fig. 5. Both area A and B are verified as amorphous with the disordered pattern. Nonetheless, at the diffraction spot (black spot) indicated by the arrow inside the area A, 0.35 nm diffraction image was observed, Fig. 5(c). This indicates the existence of crystalline graphite microstructure in the Mesh ta-C. On the other hand, no characteristic structure was observed for conventional ta-C coating, where only diffused disordered pattern observed, which indicates that it only consists of an amorphous structure.

2.3. Tribological experiments

The friction tests were performed via the cylindrical pin-on-disk tribo-tester, Fig. 6(a) under boundary lubrication regime with a constant normal load of 5, 10 and 20 N on the DLC-coated cylindrical pin, corresponds to the maximum Hertzian contact pressures of 156, 220, and 311 MPa, respectively. The cylindrical pin holder, Fig. 6(b) designed so it could create a large interference fit where it results in a large area of the cylindrical pin contact, and thus prevent the cylindrical pin from rolling during friction test. The cylindrical pin-on-disk tribo-tester method is mainly used for investigating the link between wear mechanisms, and the parameters including the contact pressure, sliding velocity, and environmental conditions. Cylindrical pin-on-disk can simulate the real line contact condition in engineering application of sliding components (main bearing, etc.) inside the engine.

The DLC-coated cylindrical pin was rubbed against an uncoated SUJ-2 disk positioned 6.65 mm eccentrically from the center of the disk under a pure sliding condition through fixing the cylindrical pin to the upper jig to prevent it from rotating. Additionally, the disk was fixed on the lower holder, which was positioned on the rotary turntable. The speed and temperature of the tests were fixed at 0.068 m/s (100 rpm) for 60 mins that correspond to 250 m of sliding distance and 80 °C, respectively (Table 1). Both cylindrical pin and counterpart disk were making sure submerged under the PAO4 oil level at which heat was applied to uphold 80 °C temperature during the friction test. The dimensions of the cylindrical pin were 5 mm in diameter and 5 mm length, whereas disk of 22.5 mm diameter and 4 mm thick were used in all experiment. In order to ensure verification and reproducibility of the findings, each friction tests were replicated three times. Liquid benzene and acetone were used as a cleaning agent in an ultrasonic bath to eliminate any contaminants on DLC-coated cylindrical pin and disk.

Wear volume loss and specific wear rates of the DLC-coated cylindrical pin were quantified via Archard wear equations by calculating the width of the worn area and assuming that the wear track is rectangular-shape Fig. 6(c) observed under the optical microscope as below:

$$k = \frac{V}{Fs} \tag{1}$$

$$V = 2l \int_{\sqrt{r^2-\left(\frac{d}{2}\right)^2}}^{r} \sqrt{r^2 - x^2}\, dx \tag{2}$$

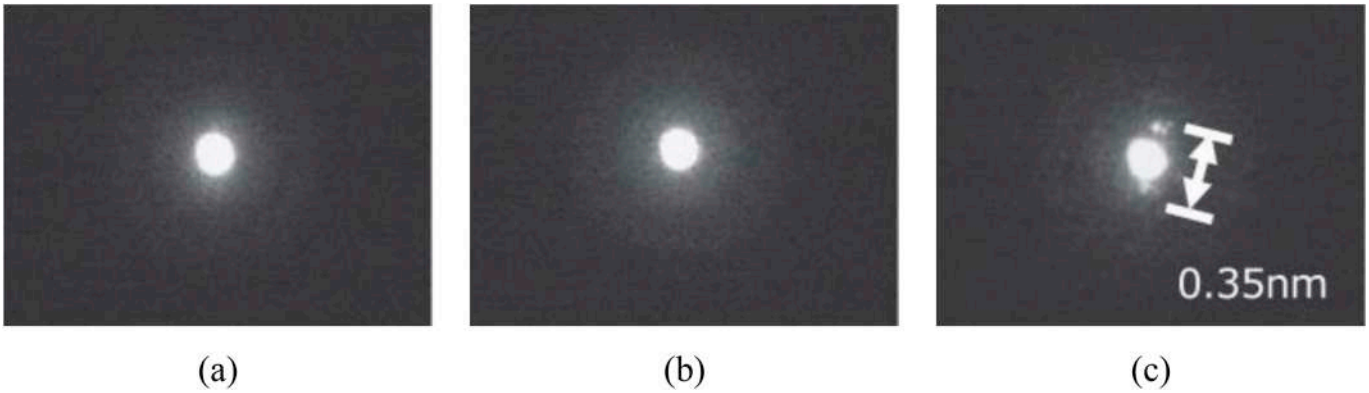

Fig. 5. Crystallinity evaluation at (a) area A, (b) area B, and (c) diffraction spot indicated by arrow inside area A [25].

Where k denotes the dimensional wear rates, F characterizes the applied normal load, s indicates the sliding distance, V symbolizes wear volume loss, d denotes the wear track width, l and r indicates the cylindrical pin length and radius, respectively.

The relation between the lambda ratio (Λ) and the minimum film thickness (h_{min}) for a rectangular shape are given by Eqn. (3), and h_{min} are quantified using Eqn. (4) [26];

$$\Lambda = \frac{h_{min}}{\sqrt{R_{q.a}^2 + R_{q.b}^2}} \tag{3}$$

$$h_{min} = 1.806(w_z')^{-0.128}(\eta_0 \tilde{u})^{0.694}\zeta^{0.568}R_x{}^{0.434} \tag{4}$$

Where;

Table 1
Friction test setup parameters.

Experimental setup	
Specimens (Cylindrical pin)	a-C:H ta-C Mesh ta-C
Specimens (Disk)	SUJ-2 Hardness: 9.9 GPa Ra: 0.01 μm
Rotation speed (m/s)	0.068
Constant normal load (N)	5, 10, 20
Temperature (°C)	80
Lubricant	PAO4
Duration (minutes)	60

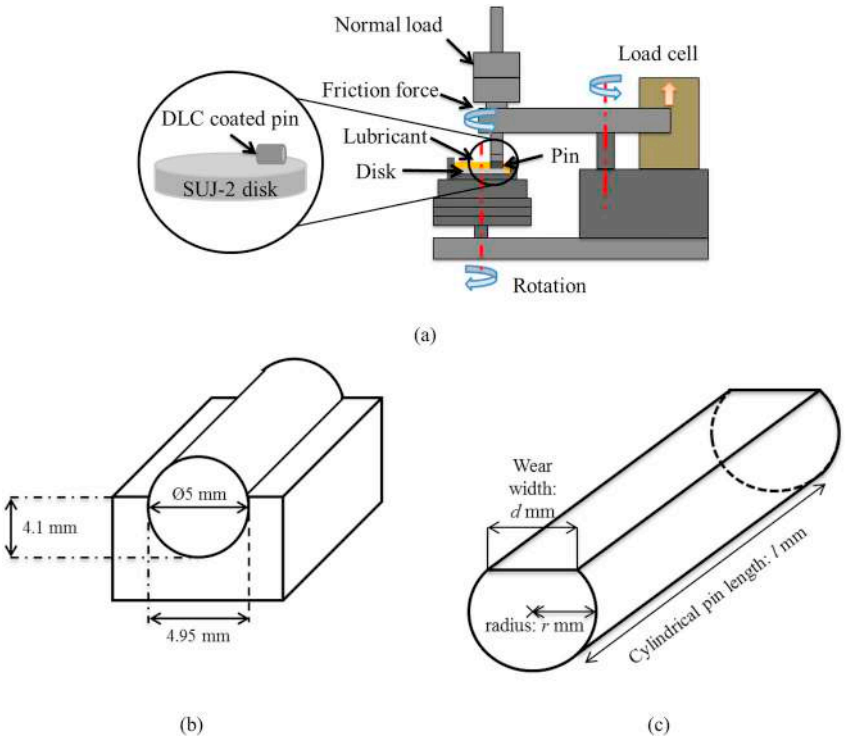

Fig. 6. (a) Tribo-tester schematic and cylindrical pin-on-disk configuration, (b) cylindrical pin holder fixture with a pin attached, and (c) schematic diagram of the worn cylindrical pin.

Table 2
Mechanical properties of the a-C:H, ta-C and Mesh ta-C coatings.

Properties	Disk	Cylindrical pin		
		a-C:H	ta-C	Mesh ta-C
Dimension (mm)	22.5 × 4	5 × 5	5 × 5	5 × 5
Substrate material	SUJ-2	SUJ-2	SUJ-2	SUJ-2
Coating method	–	CVD	PVD	PVD
Thickness (μm)	–	1.79	0.8	1.17
Elastic modulus, E_f (GPa)	275.5	97	661	232.1
Hardness, H (GPa)	9.9	14.8	78.3	27.5
Roughness, Ra (μm)	0.010	0.018	0.021	0.026

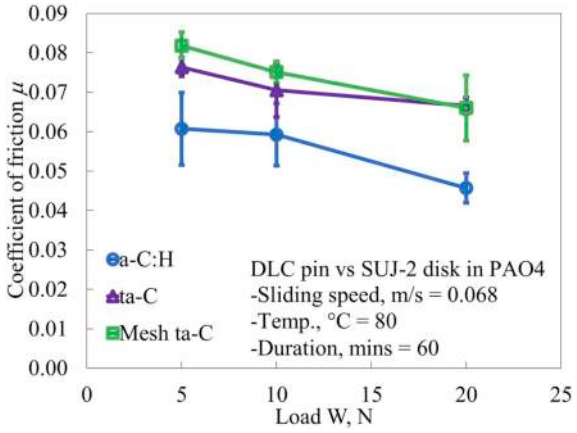

Fig. 7. CoF result for a-C:H, ta-C, and Mesh ta-C coated specimen as a function of load.

Table 3
Calculated lambda ratio Λ for a-C:H, ta-C, and Mesh ta-C coatings.

	Before friction test	After friction test
a-C:H	0.29	0.59
ta-C	0.27	0.46
Mesh ta-C	0.24	0.75

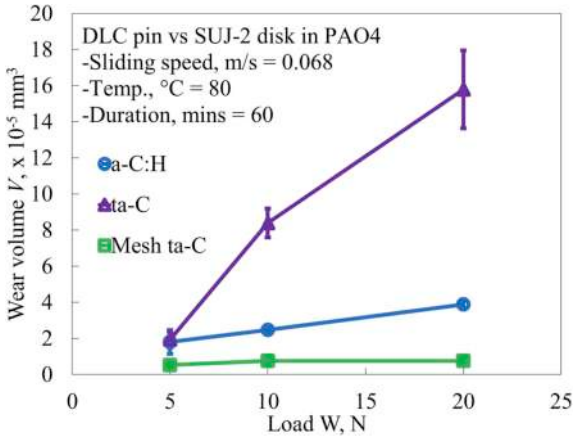

Fig. 8. Wear volumes result for a-C:H, ta-C, and Mesh ta-C coated specimen as a function of load.

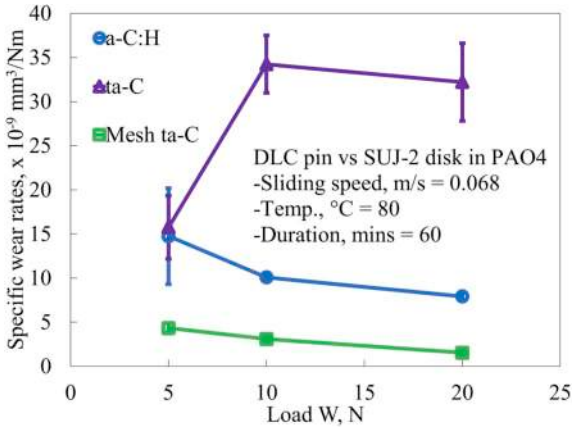

Fig. 9. Specific wear rates result for a-C:H, ta-C, and Mesh ta-C coated specimen as a function of load.

$R_{q.a}$ = roughness of the coated cylindrical pin
$R_{q.b}$ = roughness of the disk
w'_z = load per unit width (N/m)
η_0 = absolute viscosity at 0 Pa pressure and constant temperature (Pa.s)
$\bar{u}$ = mean surface velocity (m/s).
ζ = pressure-viscosity coefficient (m^2/N)
R_x = effective radius of the cylindrical pin

The calculated film parameter was less than unity which indicates that the friction tests are initially under boundary lubrication regime.

2.4. Surface analysis

NANOPICS 1000 Elionix ENT-1100a Nanoindenter was utilized to quantify hardness and Young's modulus of the DLC coatings. The surface average roughness, Ra was quantified via AFM (SPM-9700HT), and structure of the DLC was characterized by the Raman spectroscopy (NRS-1000 Laser, Jasco Inc., Japan) through laser excitation wavelength of 532 nm with detection depth of within 300–600 nm [27]. The worn area of the cylindrical pin and disk were examined by optical microscope, FE-SEM (JEOL, JSM-7000FK), and AFM. Table 2 demonstrates the mechanical properties of the DLC-coated cylindrical pin and disk.

3. Result and discussions

3.1. Friction properties for DLC films under PAO4 boundary lubrication

The coefficient of friction plotted against the load for all three distinct DLC coatings sliding on-to SUJ-2 disk in PAO4 lubrication are illustrated in Fig. 7. The CoF for Mesh ta-C was varied from 0.06 to 0.08. Furthermore, it possesses similar pattern and range as observed in ta-C results for all loads examined regardless of the high average surface roughness of the Mesh ta-C in contrast to ta-C and a-C:H. In addition, the a-C:H coating provides the lowest value of CoF at 20 N loads. Although the CoF for the Mesh ta-C is comparatively high in contrast to the a-C:H and ta-C at lower load, the CoF reduced and had approximately same results with ta-C once the load rise to 20 N. Based on the cross-sectional view of the Mesh ta-C coating as illustrated in Fig. 3 (b), the Mesh ta-C surface contains micro asperities, which is supported by the high average roughness of the coating. With the rise in load, the micro-asperities removal rates have elevated and reduced the

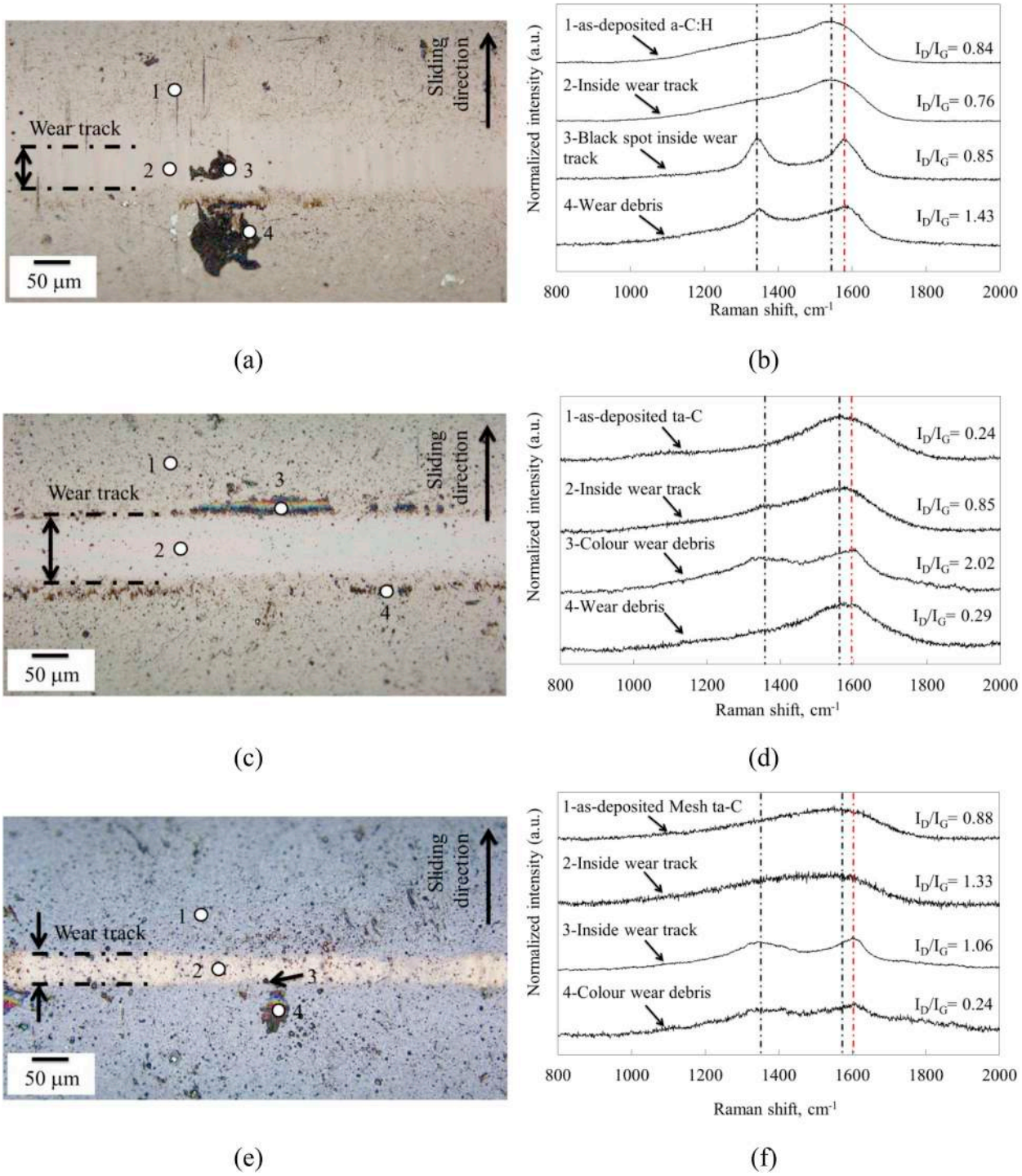

Fig. 10. Optical microscope images of the wear track on DLC coated cylindrical pin for (a) a-C:H, (c) ta-C, and (e) Mesh ta-C; and Raman spectroscopy result of the specific points for (b) a-C:H, (d) ta-C, and (f) Mesh ta-C for normal load of 20 N.

roughness of the contact surface. This leads to a smoother sliding surface as discussed in section 3.3.2. Moreover, for the a-C:H, a decrease in the CoF at higher load was linked with the formation of a graphite-like layer on the topmost surface of the wear track. This synergetic effect of the DLC and the lubrication film is further described in section 3.3.1.

There was no transition in the lubrication regime where the calculated lambda ratio Λ after the friction test is less than 1 as shown in Table 3. Since the calculated lambda ratio for every specimen used indicated that the friction test was conducted in the boundary lubrication regime, solid asperities of the coating have become the main mechanism for the improved tribological performance which dominated the contact rather than the oil film. But it is important to note that the lambda ratio measured in the case of Mesh ta-C increased to 0.75 which indicates that the friction test was approaching closer to the mixed lubrication regime. This characteristic could explain the reduction of friction coefficient result by allowing the formation of thicker oil film.

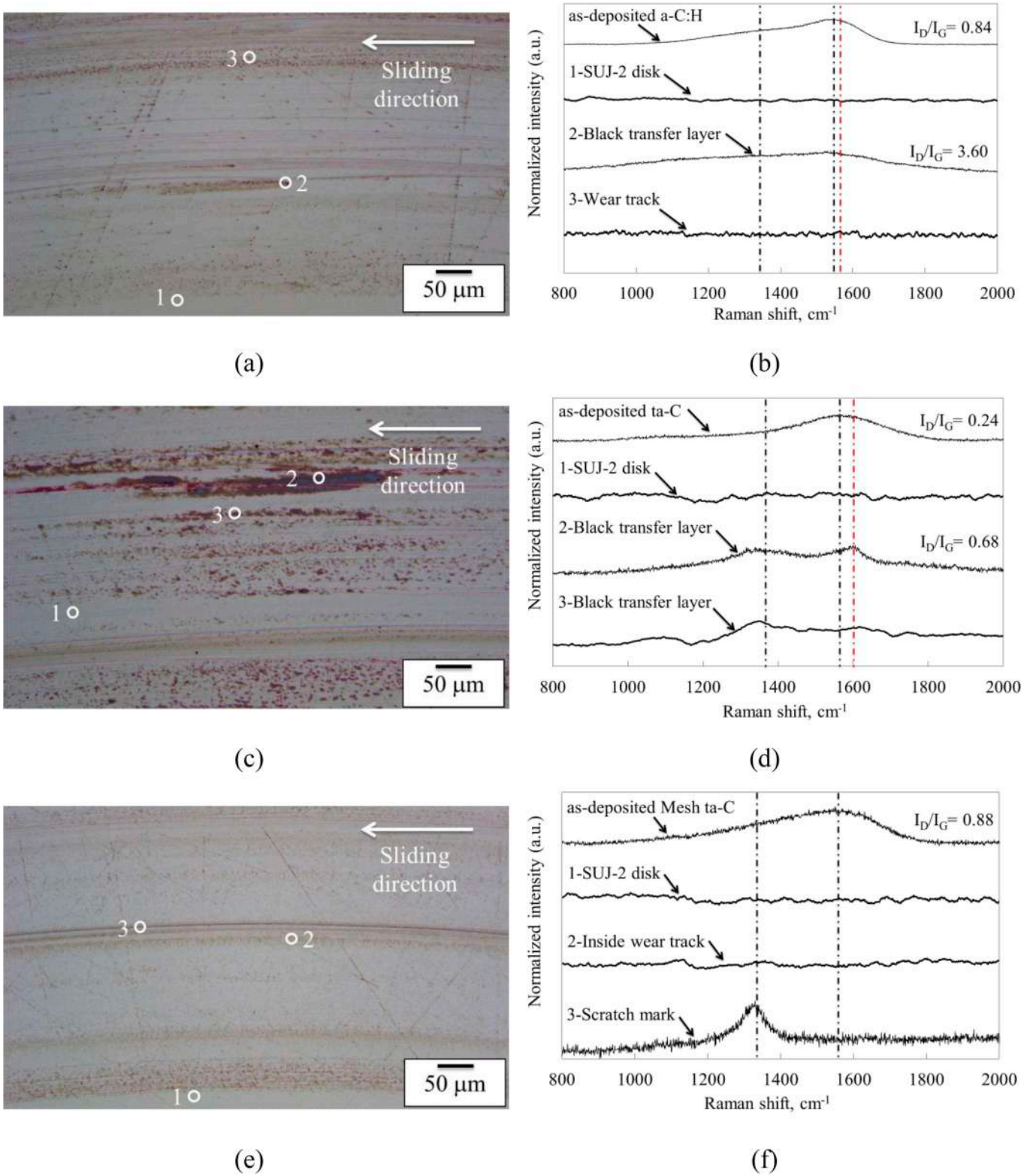

Fig. 11. Optical microscope images of the wear track on SUJ-2 disk counterpart for (a) a-C:H, (c) ta-C, and (e) Mesh ta-C; and Raman spectroscopy result of the specific points measured on the SUJ- 2 disk for (b) a-C:H, (d) ta-C, and (f) Mesh ta-C for normal load of 20 N.

3.2. Wear characteristic of DLC films in PAO4 oil under boundary lubrication

The detailed specific wear rates for every friction test were quantified on the DLC-coated cylindrical pins as to understand the influence of DLC structure on wear behaviour and respective wear mechanism of Mesh ta-C coated specimens with regard to the applied loads. Figs. 8 and 9 demonstrate the findings of wear volumes and specific wear rates for all three forms of DLC coatings towards applied normal loads. Wear volumes for all examined DLC rise with distinct rates as the normal load increased.

From the optical microscope images shown in Fig. 10, and Fig. 11,

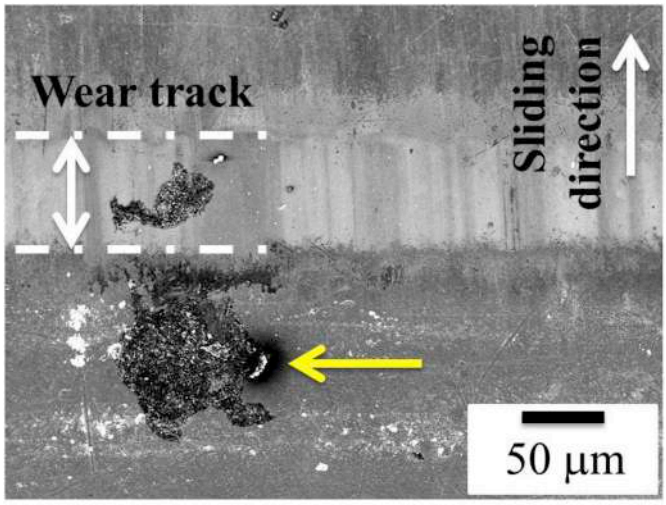

(a)

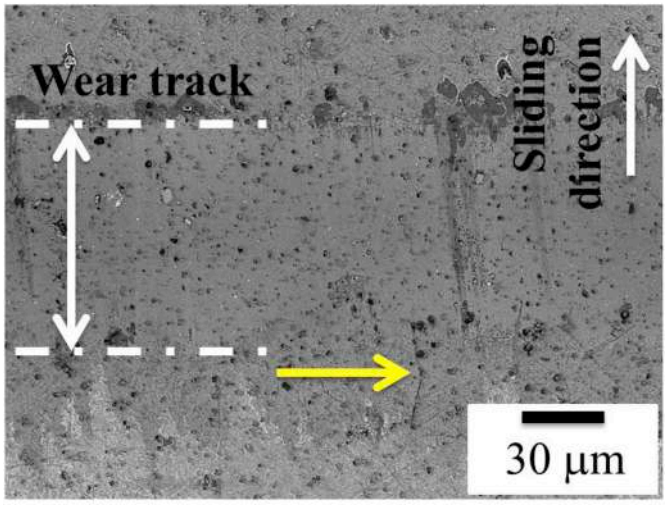

(b)

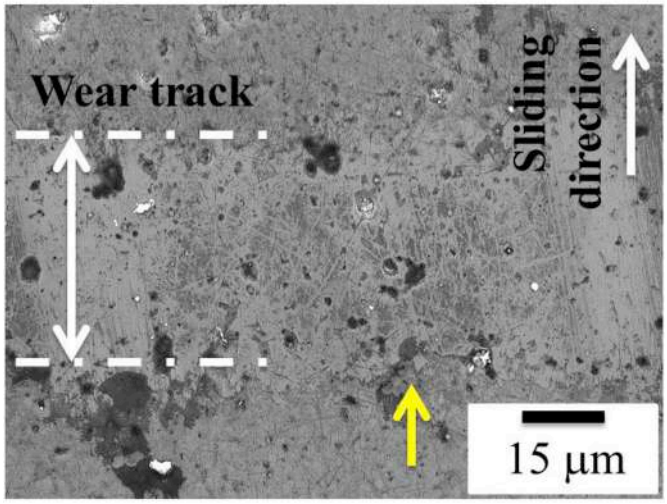

(c)

Fig. 12. FE-SEM images of the wear track on DLC coated cylindrical pin for (a) a-C:H, (b) ta-C, and (c) Mesh ta-C for normal load of 20 N.

and FE-SEM images shown in Fig. 12, there were no tribofilm derived from the oil can be detected. Since the friction test was conducted in the PAO4 base oil which characterizes by its high thermal and oxidative stability, the possibility of tribofilm derived from the oil to form is relatively low.

The worn area of a-C:H illustrates smooth surface with no formation of crack, micro-fracture or spallation inside or outside of the wear track for entire examined loads. Nonetheless, there was black wear debris left inside and adjacent to the edge of wear track as shown in Fig. 10(a). Moreover, investigation on the tribo-film was carried out by the Raman spectroscopy examination for describing the structure. The findings are elaborated in section 3.3.1. In addition, the a-C:H also had excellent wear resistant with the increase in the applied load in contrast to the ta-C.

The ta-C demonstrated severe wear with the increase in applied load, there was a linear increase in the wear volume of ta-C with the applied loads. As illustrated in Fig. 10(c), partial spalling and delamination were observed on the contact area for the ta-C coating for entire tested loads. The number of partial spalling elevated with the increase in the load. Furthermore, the colour transfer layer was observed at the edge of the wear track, which is discussed in section 3.3.1.

The Mesh ta-C demonstrated excellent wear resistance to entire applied loads. The wear rates of the Mesh ta-C specimens are extremely low (1.5–4.3 $\times$ 10^{-9} mm^3/Nm) for the entire applied loads. The wear rate of Mesh ta-C coating is approximately 21 and 5 times lesser than specific wear rates of ta-C and a-C:H coating, respectively at 20 N loads examined. It should be noted that the wear volume of Mesh ta-C had no impact on the increased applied loads. Fig. 10(e) illustrates that there is no formation of micro-crack or partial delamination on the wear track of Mesh ta-C. In some way colour tribo-layer or wear debris left near the wear track, which is elaborated in section 3.3.1.

3.3. Worn area analysis

3.3.1. Raman spectroscopy and FE-SEM analysis

Raman spectroscopy is a non-destructive instrument for depicting crystalline, nano-crystalline, and amorphous carbons. Raman spectroscopy examination was performed to quantify the alteration in the structure following the friction test. Raman spectra of disordered graphite demonstrate two quite sharp modes, the G peak almost 1580–1600 cm^{-1} and the D peak around 1350 cm^{-1}. Raman spectra are sensitive to carbon alteration, and are linked mainly to the variations of the sp^2 phase and only weakly to the sp^3 phase [28]. Two main indicators demonstrate graphitization is the increase of I_D/I_G ratio, together with the shifting of G-peak to a higher position as depicted by the red dashed line in Fig. 10(b), (d), and (f); and Fig. 11(b), and (d).

Graphitization of the DLC coating in base oil condition may occur either by the friction-induced heating under contact or high contact/shearing stress condition. However, the temperature-induced graphitization for the DLC require up to 250 °C of contact temperature to occur, and the actual contact surface temperature also reported to be 100–130 °C higher than the pre-set test temperature as a result of contact area reduction [29]. Furthermore, the transition temperature for graphitization to occur become lower with the presence of hydrogen in DLC [30–33].

The tribo-film observed in the wear track and adjacent to the edge of wear track of a-C:H was assessed by the Raman spectroscopy along with samples of ta-C, Mesh ta-C, and on every counterpart SUJ-2 disk. The quantification performed at four distinct points for DLC coated cylindrical pin, which is inside and outside of the wear track, black/colour wear debris inside and adjacent to the edge of wear track for a-C:H, ta-C, and Mesh ta-C as illustrated in Fig. 10(a), (c), and (e), respectively. Furthermore, Raman analysis performed at three points on SUJ-2 disk for each counterpart of a-C:H, ta-C, and Mesh ta-C as shown in Fig. 11(a), (c), and (e), respectively. Recent studies have shown that friction-induced graphitization at the sliding interface result in

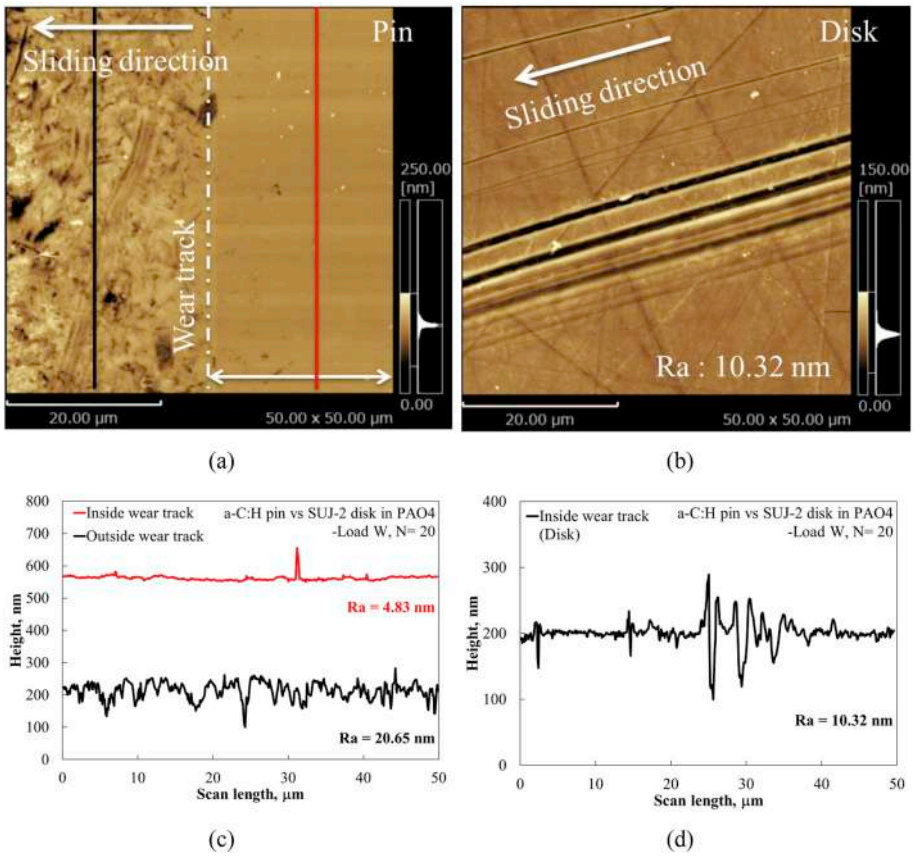

Fig. 13. AFM images of the wear track for (a) a-C:H coated cylindrical pin, and (b) SUJ-2 disk; and surface profile of the wear track for (c) a-C:H coated cylindrical pin, and (d) SUJ-2 disk for normal load of 20 N.

excellent DLC tribological performance through friction reduction and increase wear resistance [34,35]. The transferred graphite-like layer to the sliding interface can provide excellent tribological performance as a result of the synergetic effect of the lubricant and the DLC.

Raman spectrum of the black wear debris observed adjacent to the edge of wear track of the a-C:H coating indicated a remarkable rise in intensity ratio from 0.84 to 1.43 as well as shifted of G-peak position as illustrated in Fig. 10(b). This reveals graphitization of a-C:H coating. Nonetheless, there was no graphitization with regard to Raman spectrum of the black wear debris on the wear track. According to Li et al. [20], the principles wear mechanism of a-C:H coating with free-additive lubricants is graphitization beside adhesive wear. This results in the a-C:H coating to be damaged by the continuous elimination of the graphitized a-C:H layer [2,20]. Graphitization of the top surface of the a-C:H coating characterizes the decrease in CoF as the load increases. The top surface of the a-C:H coating changes to the graphite-like lamellar structure which easily sheared among layers [20,36,37]. Moreover, this graphite-like structure also transferred to the counterpart SUJ-2 disk where the Raman spectrum shows the rise in intensity ratio to 3.60 as shown in Fig. 11(b). Graphitization in a-C:H coating occurs as a result of the diffused hydrogen atom from a-C:H matrix which breaks the random covalent structure of a-C:H due to high-pressure contact condition [38,39].

Raman analysis on the wear track and outside of the wear track for ta-C likewise demonstrates no formation of graphitization as illustrated in Fig. 10(d). Nonetheless, the quantification carried out at the colour wear debris adjacent to the border of wear track demonstrates the graphitization of the ta-C coating with the rise in intensity ratio from 0.24 to 2.02. The structural alteration in ta-C was demonstrated by X. Deng et al. [40], which indicated that the graphite structure partially formed under high-temperature tribology testing. Regardless of graphitization, the ta-C coating also shows low friction and reduced wear resistance when slides against steel at a temperature of 80 °C and above as a result of thermally activated tribo-chemical interaction between carbon and ferrous atoms [9]. Optical microscope image of the SUJ-2 counterpart material of ta-C show black transferred layer on wear track as shown in Fig. 11(c). Raman analysis on this transferred layer reveals high-intensity ratio which confirms as the transferred graphitized layer from the ta-C coating during friction test as shown in Fig. 11(d). For the ta-C coating against the steel contact, abrasive wear was observed on the sliding surface when lubricated with PAO4 and the coatings gradually damaged through brittle micro-fracture in the protruding part, which then advances to spalling and delamination of the coatings [8,10,41,42].

Fig. 10(f) demonstrates the finding of the Mesh ta-C Raman analysis, where the as-deposited structure was formed in combination of sp^2 and sp^3 phase. Furthermore, the quantification carried out inside the wear track illustrates that the I_D/I_G ratio elevated from 0.88 to 1.33. This characterizes the structural transformation to higher intensity graphitization. Therefore, regardless of the alteration in the average roughness of the as-deposited Mesh ta-C, graphitization process could also characterize the CoF reduction. Furthermore, the increase in the intensity ratio does not affect the wear performance of Mesh ta-C as can be observed in the case of a-C:H coating. The Mesh ta-C could prevent the shearing of the graphite-like layer formed on the rubbing surface which results in high wear resistance of the coating. Additionally, the Raman analysis conducted on the SUJ-2 disk counterpart material Fig. 11(f) shows no evidence of graphite-like structure being transferred as what can be observed in the case of a-C:H and ta-C coating. However, Raman analysis on the scratch mark observed on the SUJ-2 disk Fig. 11(e) shows only a D-peak, which can be explained as the oxidize hematite (α-Fe_2O_3) phases at 290 and 1310 cm^{-1} peak position

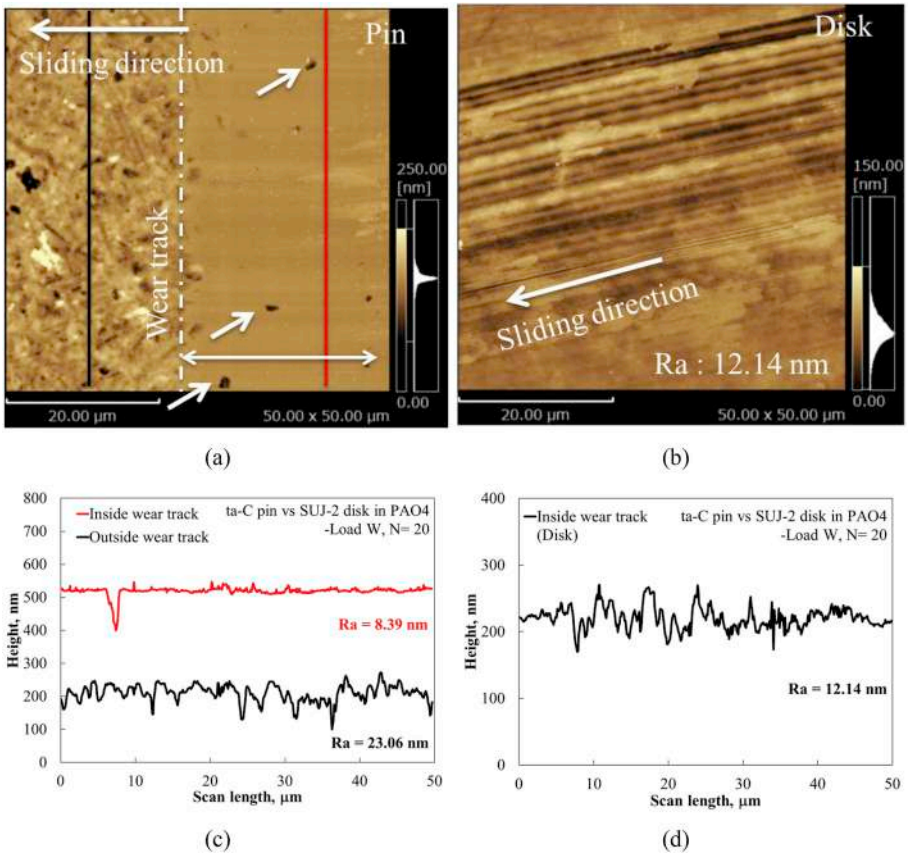

Fig. 14. AFM images of the wear track for (a) ta-C coated cylindrical pin, and (b) SUJ-2 disk; and surface profile of the wear track for (c) ta-C coated cylindrical pin, and (d) SUJ-2 disk for normal load of 20 N.

[22,43–46].

The wear track of the a-C:H as observed by the FE-SEM image Fig. 12(a), demonstrates a smooth surface lacking any deep scratch owing to abrasive action by wear particle. Neither inside the wear track nor outside wear track demonstrates any indication of micro-crack or fracture. Furthermore, this also demonstrates that there was no spalling or delamination observed on the wear track of the a-C:H.

On the other hand, the FE-SEM image for ta-C Fig. 12(b), and Fig. 16(b) demonstrates brittle micro-crack inside and near to the edge of wear track. This micro-crack turns into severe and propagates to the edge of wear track when the load is elevated. Based on FE-SEM image, it is well-established that the crack is a through thickness crack, which then results in the spalling out and delamination of the coatings that functions as the abrasive wear particles that quicken the wear. The findings of the wear track for the friction test of 10 N loads as illustrated in Fig. 16(b) also indicates numerous micro-cracks that propagate and impair the coating. In contrast, the crack is evident at the edge of wear track at 20 N loads, Fig. 12(b). This phenomenon is characterized by the wear volumes of the ta-C that is nearly at the worn out phase.

With regard to Mesh ta-C, the presence of several areas along the wear track demonstrates the non-uniform wear track width. This could be the consequence of the plastic deformation for wear of ductile material [47]. In addition, there were no delamination observed inside the wear track of Mesh ta-C. Nonetheless, micro-cracks were observed adjacent to the spot where spalling occurs, Fig. 12(c) as observed by FE-SEM. The crack has been shown to lead to the partial spallation of the coatings. Nevertheless, this micro-crack is not a category of through-thickness crack as it leads to partial spalling without any indication of coating delamination.

3.3.2. AFM analysis of worn surface

In order to elucidate the wear mechanism and behaviour of a-C:H, ta-C, and Mesh ta-C, the surface examination was performed on the wear track of both DLC coated cylindrical pin and SUJ-2 disk by AFM. The measurement areas were fixed at 50 × 50 µm as to capture the surface of inside and outside of wear track. Figs. 13–15 demonstrate the findings of AFM quantification on both coated cylindrical pin and disk surface for a-C:H, ta-C, and Mesh ta-C respectively after 1-h friction test at 20 N loads. For the a-C:H as illustrated in Fig. 13(a), smoothening of the surface of wear track is evident in contrast to as deposited. Besides that, the surface profile is illustrated in Fig. 13(c) where the average roughness of a-C:H wear track decreased by 76% to 4.83 nm. On the other hand, the counterpart material SUJ-2 disk as shown in Fig. 13(b) indicates the scratch mark at numerous contact points with the quantified average surface roughness of 10.32 nm.

Examination of the ta-C coated cylindrical pin indicates numerous spots with spallation of the coating and also several deep grooves were observed on the wear track as demonstrated in Fig. 14(a). The surface profile of ta-C coated cylindrical pin wear track as illustrated in Fig. 14(c) is rougher in contrast to a-C:H with an average roughness of 8.39 nm. Whereas the SUJ-2 disk also demonstrates clear deep grooves marks with an average roughness of 12.14 nm as in Fig. 14(d). This verifies the spalling fragments of ta-C accumulated at the mating surface and functions as abrasive particles causing a severe scratch on the SUJ-2 mating surface. Combination of the micro-crack of the ta-C coating as described in section 3.3.1, spalling and abrasion by the mounted up ta-C fragments cause severe wear of the coating. Since ta-C is harder in contrast to SUJ-2 steel disk, it produces rough abrasive wear scratch lines corresponding to the sliding direction by means of the fragments of abrasive particles. Tasdemir et al. [24] demonstrated that wear behaviour of the ta-C cylindrical pin lubricated with PAO4

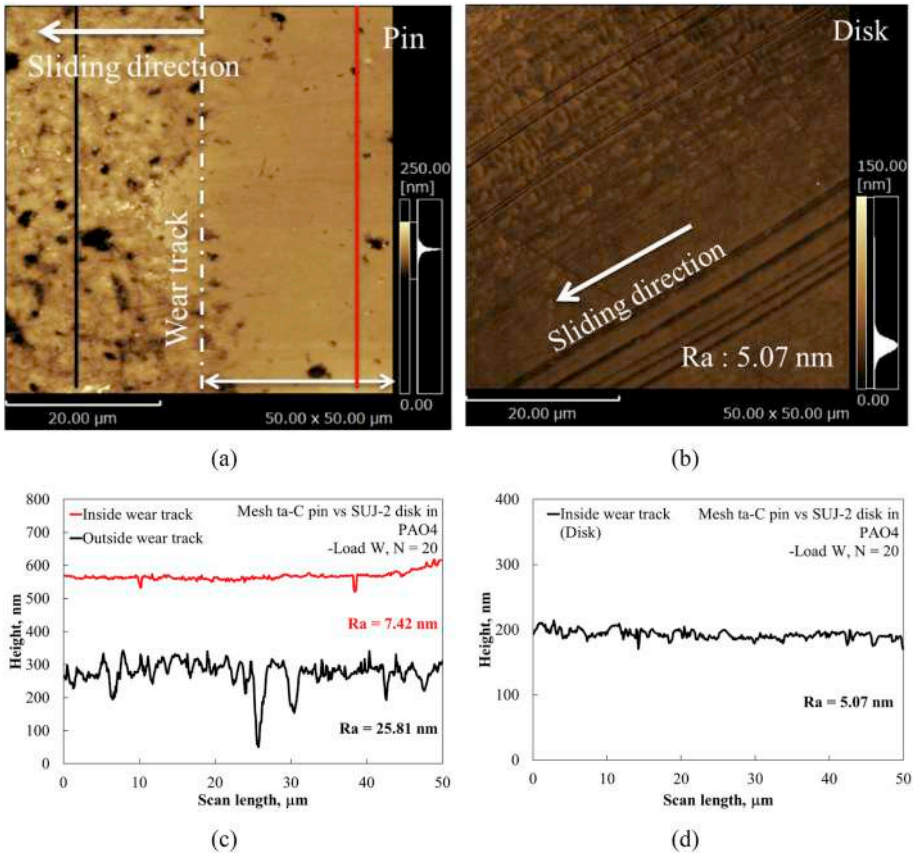

Fig. 15. AFM images of the wear track for (a) Mesh ta-C coated cylindrical pin, and (b) SUJ-2 disk; and surface profile of the wear track for (c) Mesh ta-C coated cylindrical pin, and (d) SUJ-2 disk for normal load of 20 N.

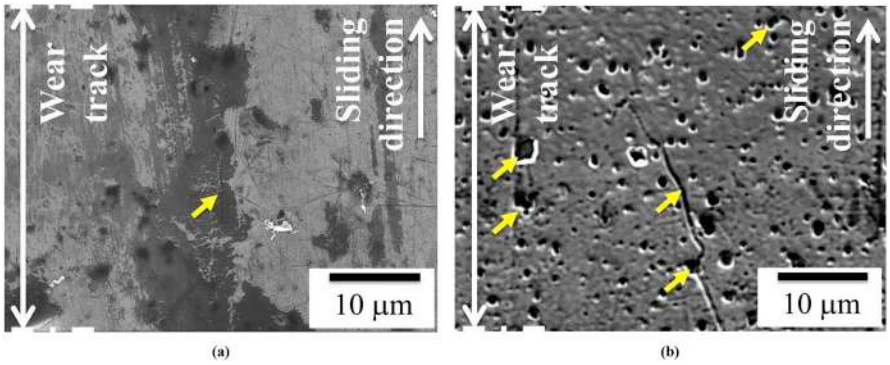

Fig. 16. FE-SEM images of the wear track for (a) Mesh ta-C coated cylindrical pin, and (b) ta-C coated cylindrical pin for an applied normal load of 10 N.

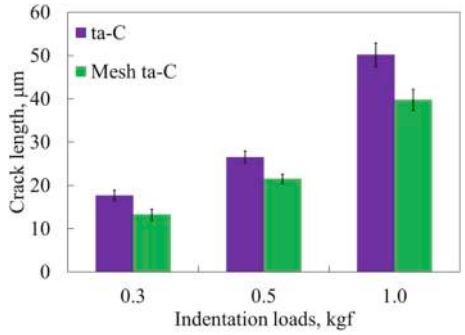

Fig. 17. Radial crack length measured after indentation test under 0.3, 0.5, and 1.0 kgf loads.

indicated that wear occurs as polishing for DLC/steel contact.

For the Mesh ta-C, the wear track average roughness reduced nearly 3.5 times to 7.42 nm. The surface profiles of the wear track quantified on the Mesh ta-C coated cylindrical pin also indicates smoothers surface in contrast to as deposited Mesh ta-C as illustrated in Fig. 15(a), and (c). Further examination on the mating material SUJ-2 disk exposes polishing effects that decrease the disk roughness by 2 times from 10 nm to 5.07 nm as illustrated in Fig. 15(b), and (d). The profile of the wear track on the SUJ-2 disk had less deep scratch marks owing to hard abrasive particles generated during friction test. Thus, friction reduction in Mesh ta-C was largely contributed by the surface smoothening which increases the lambda value from 0.24 to 0.75 after the friction test. This would favour the friction reduction by allowing the formation of thicker oil film. Surface enhancement by solid nanoparticles has been reported to play an important effect that would reduce the friction and provide high wear resistance through interaction on the sliding surface

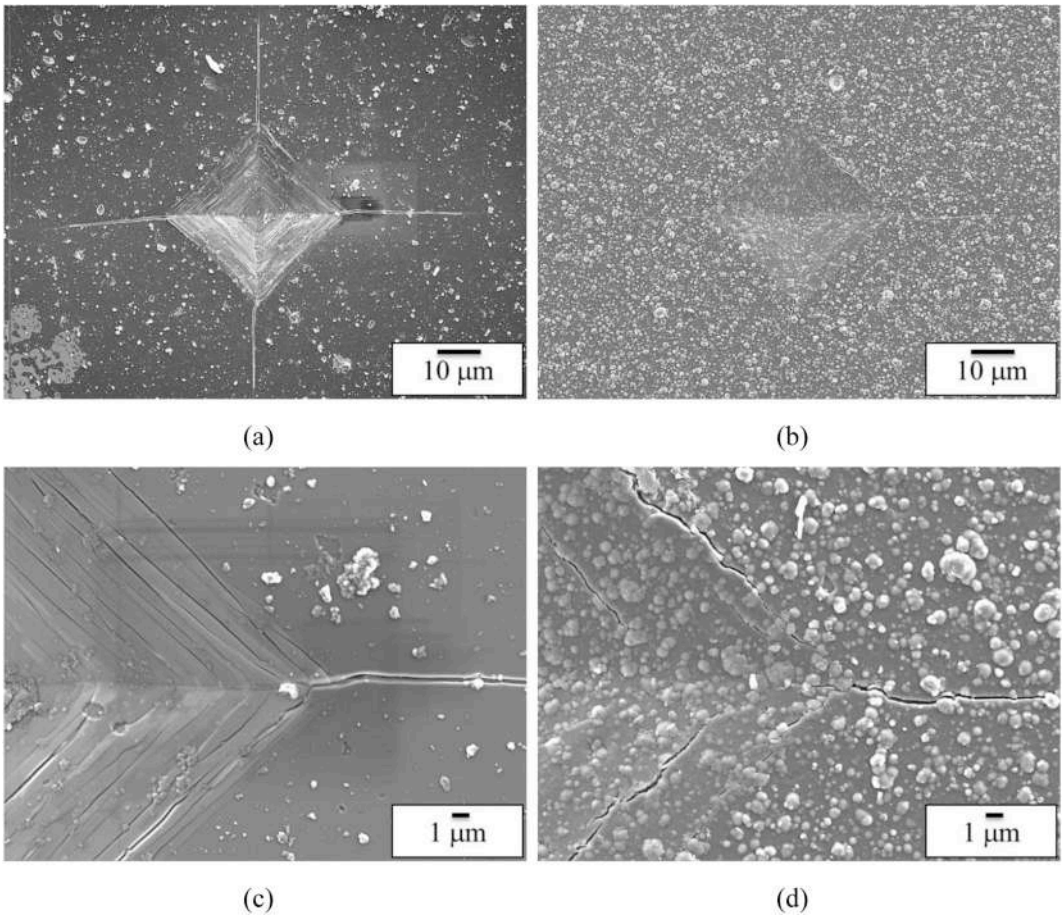

Fig. 18. FE-SEM images of indentation mark and radial crack formed on (a) ta-C, and (b) Mesh ta-C coatings; and magnified indentation mark of (c) ta-C, and (d) Mesh ta-C for 1.0 kgf indentation loads.

[48]. But for the case of additive-free lubricant, surface enhancement could be achieved by controlling the amount and size of abrasive particle produce during the friction test. Thus, the wear mechanism of the Mesh ta-C could be described through the inhibition of micro-crack of the coating which subsequently prevents the generation of high hardness abrasive particles.

3.4. Crack resistance of the Mesh ta-C

The Mesh ta-C that is made up of sp^2-rich mesh structure offers excellent wear resistance despite the fact that the hardness of the Mesh ta-C coating is nearly three times lesser than the hardness of ta-C coatings. The advantages of the Mesh ta-C can be explained by the hardness, which increased along the coating depth from the topmost surface to the substrate. This leads to prevention of the coating failures due to brittle micro-crack that result in coating spalling out and delamination. C. Charitidis et al. demonstrated that layered structure (sequence of soft/hard carbon layers) causing thick, stable and sp^3 rich films demonstrates improved adhesion strength in contrast to those that are rich in sp^2 content. This could sustain coating cracking without debonding. Layered structure coatings display nearly full elastic response, while on films rich in sp^2 content demonstrates massive brittle fragmentation [49].

As illustrated in Fig. 16(a), the Mesh ta-C coating lacks any brittle cracking and micro-fracture. Only a tiny scratch without any evidence of spalling and delamination can be observed. Moreover, the coating can be considered for transforming elastically in order to absorb the friction force during the test. Nonetheless, it is clear that crack is formed on the ta-C cylindrical pin even at lower load, Fig. 16(b). The brittle type cracking observed on the cylindrical pin caused micro spalling and delamination, which formed high hardness fragments that abrasively accelerate the wear.

To further clarifying high crack resistance of Mesh ta-C as compared to the ta-C coating, micro-indentation test was conducted on both types of coating deposited on the Si-substrate. Radial crack length was measured from the center of the indentation mark to the crack tip. The result of the radial crack length was simplified in Fig. 17 by averaging the crack length of 6 indentations test. The micro-indentation test was only performed on the ta-C and Mesh ta-C specimens, since a-C:H coating wear mechanism does not involve micro-fracture as discussed earlier in section 3.3.1.

Mesh ta-C demonstrate the shortest radial crack length for all indentation loads applied as compared to the ta-C, revealing poor fracture toughness of ta-C coating. By introducing the structure to the ta-C, the fracture toughness of the coating increased, and thus could prevent the crack propagation that progress into spalling and delamination of the coating. The soft structure sp^2 phase terminates the crack propagation through energy release by plastic deformation leads to film toughness enhancement [50]. This is supported by the latest finding by X. Sui et al. [51] which reported that high crack propagation resistance and elastic recovery capability through multilayer design of hard and soft film result in excellent tribological performance. Moreover, increased of elastic recovery by means of reducing the plastic deformation area result in improved coating toughness [52,53].

Fig. 18(a), and (b) shows the FE-SEM images of the indentation mark on the ta-C and Mesh ta-C coating, respectively. It is evidenced that the diagonal length of the indentation mark on ta-C and Mesh ta-C is identical even though the ta-C is harder than Mesh ta-C. Furthermore,

investigation of the radial crack and the indentation mark reveal different crack type between ta-C and Mesh ta-C. The radial crack formed on ta-C coating is finer as compared to radial crack formed on Mesh ta-C sample. The ta-C coating also demonstrates a fine layer cracking pattern inside the indentation mark as shown in Fig. 18(c), which is explained by the inability of the coating to undergo elastic/plastic deformation under loading condition. A large amount of transverse cracks in and around the indentation mark can be observed due to high hardness and brittle characteristic of ta-C coating.

Moreover, investigation of the indentation mark of Mesh ta-C coating shows a distinct crack type where each crack was not connected as shown in Fig. 18(d). This proves the hypothesis that the Mesh ta-C undergoes elastic/plastic deformation to absorb the induced tensile stress upon loadings, which result in ductile cracking. The intersection effect and soft sp^2 structure could restraint the crack propagation in Mesh ta-C. In addition, the as-deposited Mesh ta-C top surface form in a combination of sp^2 and sp^3 carbon phase as compared to the only sp^3 exist in conventional ta-C. This feature has been reported to provide high toughness coating with a relatively low hardness as the sp^3 contents reduce [53].

4. Conclusion

The current study examined the effect of mesh structure DLC coating on tribological performance, particularly with regard to friction and wear in base-oil lubrication conditions. The findings of the friction test revealed that the Mesh ta-C had a similar pattern and value of the friction coefficient to that of ta-C. Apart from that, there were no graphitized transferred-film found on the SUJ-2 disk for Mesh ta-C which detected on SUJ-2 disk for a-C:H and ta-C coatings mating material. Mesh ta-C friction reduction is explained by the surface smoothening due to polishing effect. With regard to wear, the Mesh ta-C offers excellent wear resistance in contrast to the a-C:H and ta-C. Furthermore, specific wear rates of the Mesh ta-C at high load decreased by 93% in contrast to the ta-C at a nearly similar coefficient of friction. Raman analysis of the Mesh ta-C and its counterpart worn area shows the reduction of wear effect due to the formation of graphite-like structure on the contact surface. Examination of the wear track of the Mesh ta-C coated cylindrical pin demonstrates the deterrence of crack initiation and propagation, where there was a lack of evidence pertaining to cracks in contrast to the ta-C. Mesh ta-C could sustain the induced tensile stress by elastic/plastic deformations. Moreover, less amount and size of high hardness abrasive particles generated also contributes to the high wear resistance of Mesh ta-C which is verified through reduction of the as-manufactured average roughness, Ra of counterpart material. This result in increased lambda value which allows the formation of thicker oil film. As for ta-C coating, brittle micro-fracture was observed, that progresses to partial spalling and functions as the high hardness abrasive particles to accelerate the wear. Whereas, the a-C:H wear mechanism is elucidated by the progressive elimination of the graphitized contact surface causing high wear and low friction coefficient. Hence, the Mesh ta-C indicates excellent wear resistance owing to inhibition of microfracture and cracks propagation by the structure together with the reduction of abrasive particle production. On the other hand, the ta-C and a-C:H endured abrasive wear due to microcrack and graphitization-induced wear mechanism, respectively.

Acknowledgment

The author would like to thank Ministry of Higher Education, Malaysia and Universiti Teknikal Malaysia Melaka for their financial support.

Appendix A. Supplementary data

Supplementary data to this article can be found online at https://doi.org/10.1016/j.triboint.2019.01.016.

References

[1] Dobrenizki L, Tremmel S, Wartzack S, Hoffmann DC, Brögelmann T, Bobzin K, et al. Efficiency improvement in automobile bucket tappet/camshaft contacts by DLC coatings – influence of engine oil, temperature and camshaft speed. Surf Coating Technol 2016. https://doi.org/10.1016/j.surfcoat.2016.09.041.
[2] Ronkainen H, Varjus S, Koskinen J, Holmberg K. Differentiating the tribological performance of hydrogenated and hydrogen-free DLC coatings. Wear 2001;249:260–6. https://doi.org/10.1016/S0043-1648(01)00558-0.
[3] Kato K. Wear in relation to friction - a review. Wear 2000;241:151–7. https://doi.org/10.1016/S0043-1648(00)00382-3.
[4] Halling J. The tribology of surface films. Thin Solid Films 1983;108:103–15. https://doi.org/10.1016/0040-6090(83)90496-0.
[5] Polaki SR, Kumar N, Ganesan K, Madapu K, Bahuguna A, Kamruddin M, et al. Tribological behavior of hydrogenated DLC film: chemical and physical transformations at nano-scale. Wear 2015;338–339:105–13. https://doi.org/10.1016/j.wear.2015.05.013.
[6] Tasdemir HA, Tokoroyama T, Kousaka H, Umehara N, Mabuchi Y. Friction and wear performance of boundary-lubricated DLC/DLC contacts in synthetic base oil. Procedia Eng 2013;68:518–24. https://doi.org/10.1016/j.proeng.2013.12.215.
[7] Masuko M, Ono T, Aoki S, Suzuki A, Ito H. Friction and wear characteristics of DLC coatings with different hydrogen content lubricated with several Mo-containing compounds and their related compounds. Tribol Int 2015;82:350–7. https://doi.org/10.1016/j.triboint.2014.04.037.
[8] Semenov a P, Khrushchov MM. Influence of environment and temperature on tribological behavior of diamond and diamond-like coatings. J Frict Wear 2010;31:142–58. https://doi.org/10.3103/S106836661002008X.
[9] Abdullah Tasdemir H, Wakayama M, Tokoroyama T, Kousaka H, Umehara N, Mabuchi Y, et al. The effect of oil temperature and additive concentration on the wear of non-hydrogenated DLC coating. Tribol Int 2014;77:65–71. https://doi.org/10.1016/j.triboint.2014.04.015.
[10] Al Mahmud KAH, Varman M, Kalam MA, Masjuki HH, Mobarak HM, Zulkifli NWM. Tribological characteristics of amorphous hydrogenated (a-C: H) and tetrahedral (ta-C) diamond-like carbon coating at different test temperatures in the presence of commercial lubricating oil. Surf Coating Technol 2014;245:133–47. https://doi.org/10.1016/j.surfcoat.2014.02.052.
[11] Kalin M, Vižintin J, Barriga J, Vercammen K, van Acker K, Arnšek A. The effect of doping elements and oil additives on the tribological performance of boundary-lubricated DLC/DLC contacts. Tribol Lett 2004;17:679–88. https://doi.org/10.1007/s11249-004-8073-1.
[12] Vengudusamy B, Mufti RA, Lamb GD, Green JH, Spikes HA. Friction properties of DLC/DLC contacts in base oil. Tribol Int 2011;44:922–32. https://doi.org/10.1016/j.triboint.2011.03.006.
[13] Podgornik B, Jacobson S, Hogmark S. DLC coating of boundary lubricated components - advantages of coating one of the contact surfaces rather than both or none. Tribol Int 2003;36:843–9. https://doi.org/10.1016/S0301-679X(03)00102-6.
[14] Topolovec-Miklozic K, Lockwood F, Spikes H. Behaviour of boundary lubricating additives on DLC coatings. Wear 2008;265:1893–901. https://doi.org/10.1016/j.wear.2008.04.051.
[15] Abdullah Tasdemir H, Wakayama M, Tokoroyama T, Kousaka H, Umehara N, Mabuchi Y, et al. Ultra-low friction of tetrahedral amorphous diamond-like carbon (ta-C DLC) under boundary lubrication in poly alpha-olefin (PAO) with additives. Tribol Int 2013;65:286–94. https://doi.org/10.1016/j.triboint.2013.03.014.
[16] Liu X, Yamaguchi R, Umehara N, Deng X, Kousaka H, Murashima M. Clarification of high wear resistance mechanism of ta-CNx coating under poly alpha-olefin (PAO) lubrication. Tribiology Int 2017;105:193–200. https://doi.org/10.1016/j.triboint.2016.10.016.
[17] Herdan JM. Lubricating oil additives and the environment - an overview. Lubric Sci 1997;9:161–72. https://doi.org/10.1002/ls.3010090205.
[18] Moore MA, King FS. Abrasive wear of brittle solids. Wear 1980;60:123–40. https://doi.org/10.1016/0043-1648(80)90253-7.
[19] Bull SJ. Tribology of carbon coatings: DLC, diamond and beyond. Diam Relat Mater 1995;4:827–36. https://doi.org/10.1016/0925-9635(94)05325-1.
[20] Li X, Deng X, Kousaka H, Umehara N. Comparative study on e ff ects of load and sliding distance on amorphous hydrogenated carbon (a-C : H) coating and tetrahedral amorphous carbon (ta- C) coating under base-oil lubrication condition. Wear 2017;392–393:84–92. https://doi.org/10.1016/j.wear.2017.09.009.
[21] Van der Donck T, Muchlado M, Zein Eddine W, Achanta S, Carvalho NJM, Celis JP. Effect of hydrogen content in a-C:H coatings on their tribological behaviour at room temperature up to 150 °C. Surf Coating Technol 2009;203:3472–9. https://doi.org/10.1016/j.surfcoat.2009.05.032.
[22] Wong PL, He F, Zhou X. Interpretation of the hardness of worn DLC particles using micro-Raman spectroscopy. Tribol Int 2010;43:1806–10. https://doi.org/10.1016/j.triboint.2010.04.008.
[23] Bewilogua K, Hofmann D. History of diamond-like carbon films - from first experiments to worldwide applications. Surf Coating Technol 2014;242:214–25. https://doi.org/10.1016/j.surfcoat.2014.01.031.
[24] Tasdemir HA, Wakayama M, Tokoroyama T, Kousaka H, Umehara N, Mabuchi Y, et al. Wear behaviour of tetrahedral amorphous diamond-like carbon (ta-C DLC) in additive containing lubricants. Wear 2013;307:1–9. https://doi.org/10.1016/j.wear.2013.08.011.
[25] Moriguchi H, Shibata A, Watanabe J. Tribological properties of new type DLC film

"Geniuscoat HAM" Nissin Electr Rev 2017;62.
[26] Hamrock BJ, Schmid SR, Jacobson BO. Fundamentals of fluid film lubrication. CRC Press; 2004.
[27] Harima H. UV-Raman observation of Si surface layer with very shallow ion-implantation. Kenbikyo 2008;43:133–6.
[28] Ferrari AC, Robertson J. Interpretation of Raman spectra of disordered and amorphous. Carbon 2000;61:95–107.
[29] Kalin M, Vižintin J. Real contact temperatures as the criteria for the reactivity of diamond-like-carbon coatings with oil additives. Thin Solid Films 2010;518:2029–36. https://doi.org/10.1016/j.tsf.2009.08.055.
[30] Bremond F, Fournier P, Platon F. Test temperature effect on the tribological behavior of DLC-coated 100C6-steel couples in dry friction. Wear 2003;254:774–83. https://doi.org/10.1016/S0043-1648(03)00263-1.
[31] Tallant DR, Parmeter JE, Siegal MP, Simpson RL. The thermal stability of diamond-like carbon. Diam Relat Mater 1995;4:191–9. https://doi.org/10.1016/0925-9635(94)00243-6.
[32] Ogwu AA, Lamberton RW, Morley S, Maguire P, McLaughlin J. Characterization of thermally annealed diamond like carbon (DLC) and silicon modified DLC films by Raman spectroscopy. Phys B Condens Matter 1999;269:335–44. https://doi.org/10.1016/S0921-4526(99)00138-6.
[33] Erdemir A, Donnet C. Tribology of diamond-like carbon films: recent progress and future prospects. J Phys D Appl Phys 2006;39. https://doi.org/10.1088/0022-3727/39/18/R01.
[34] Zhuang W, Fan X, Li W, Li H, Zhang L, Peng J, et al. Comparing space adaptability of diamond-like carbon and molybdenum disulfide films toward synergistic lubrication. Carbon N Y 2018;134:163–73. https://doi.org/10.1016/j.carbon.2018.03.059.
[35] Li W, Fan X, Li H, Zhu M, Wang L. Probing carbon-based composite coatings toward high vacuum lubrication application. Tribol Int 2018;128:386–96. https://doi.org/10.1016/j.triboint.2018.07.043.
[36] Liu Y, Erdemir A, Meletis EI. A study of the wear mechanism of diamond-like carbon films 1. Surf Coating Technol 1996;82:48–56. https://doi.org/10.1016/0257-8972(95)02623-1.
[37] Liu Y, Erdemir A, Meletis EI. An investigation of the relationship between graphitization and frictional behavior of DLC coatings. Surf Coating Technol 1996;86–87:564–8. https://doi.org/10.1016/S0257-8972(96)03057-5.
[38] Kosarieh S, Morina A, Lainé E, Flemming J, Neville A. Tribological performance and tribochemical processes in a DLC/steel system when lubricated in a fully formulated oil and base oil. Surf Coating Technol 2013;217:1–12. https://doi.org/10.1016/j.surfcoat.2012.11.065.
[39] Voevodin AA, Phelps AW, Zabinski JS, Donley MS. Friction induced phase transformation of pulsed laser deposited diamond-like carbon. Diam Relat Mater 1996;5:1264–9.
[40] Deng X, Kousaka H, Tokoroyama T, Umehara N. Tribological behavior of tetrahedral amorphous carbon (ta-C) coatings at elevated temperatures. Tribol Int 2014;75:98–103. https://doi.org/10.1016/j.triboint.2014.04.002.
[41] Mabuchi Y, Higuchi T, Inagaki Y, Kousaka H, Umehara N. Wear analysis of hydrogen-free diamond-like carbon coatings under a lubricated condition. Wear 2013;298–299:48–56. https://doi.org/10.1016/j.wear.2012.11.046.
[42] Masripan NA Bin, Ohara K, Umehara N, Kousaka H, Tokoroyama T, Inami S, et al. Hardness effect of DLC on tribological properties for sliding bearing under boundary lubrication condition in additive-free mineral base oil. Tribol Int 2013;65:265–9. https://doi.org/10.1016/j.triboint.2013.01.016.
[43] Mabuchi Y, Higuchi T, Weihnacht V. Effect of sp2/sp3 bonding ratio and nitrogen content on friction properties of hydrogen-free DLC coatings. Tribol Int 2013;62:130–40. https://doi.org/10.1016/j.triboint.2013.02.007.
[44] Komori K, Umehara N. Effect of surface morphology of diamond-like carbon coating on friction, wear behavior and tribo-chemical reactions under engine-oil lubricated condition. Tribol Int 2015;84:100–9. https://doi.org/10.1016/j.triboint.2014.11.010.
[45] Park SJ, Lee KR, Ko DH. Tribological behavior of nano-undulated surface of diamond-like carbon films. Diam Relat Mater 2005;14:1291–6. https://doi.org/10.1016/j.diamond.2004.07.021.
[46] Abdollah MF Bin, Yamaguchi Y, Akao T, Inayoshi N, Umehara N, Tokoroyama T. Phase transformation studies on the a-C coating under repetitive impacts. Surf Coating Technol 2010;205:625–31. https://doi.org/10.1016/j.surfcoat.2010.07.062.
[47] Moore MA, King FS. Abrasive wear of brittle solids* 1980;60:123–40.
[48] Fan X, Wang L, Li W, Wan S. Improving tribological properties of multialkylated cyclopentanes under simulated space environment: two feasible approaches. ACS Appl Mater Interfaces 2015;7:14359–68. https://doi.org/10.1021/acsami.5b03088.
[49] Charitidis C, Logothetidis S, Gioti M. A comparative study of the nanoscratching behavior of amorphous carbon films grown under various deposition conditions 125. 2000. p. 201–6.
[50] Subramanian C, Strafford KN. Review of multicomponent and multilayer coatings for tribological applications. Wear 1993;165:85–95. https://doi.org/10.1016/0043-1648(93)90376-W.
[51] Sui X, Liu J, Zhang S, Yang J, Hao J. Microstructure, mechanical and tribological characterization of CrN/DLC/Cr-DLC multilayer coating with improved adhesive wear resistance. Appl Surf Sci 2018;439:24–32. https://doi.org/10.1016/j.apsusc.2017.12.266.
[52] Zhang JY, Liu G, Zhang X, Zhang GJ, Sun J, Ma E. A maximum in ductility and fracture toughness in nanostructured Cu/Cr multilayer films. Scripta Mater 2010;62:333–6. https://doi.org/10.1016/j.scriptamat.2009.10.030.
[53] Guo CQ, Pei ZL, Fan D, Gong J, Sun C. Microstructure and tribomechanical properties of (Cr, N)-DLC/DLC multilayer films deposited by a combination of filtered and direct cathodic vacuum arcs. Diam Relat Mater 2015;60:66–74. https://doi.org/10.1016/j.diamond.2015.10.019.